Long-term sea surface temperature and climate change in the Australian–New Zealand region

Timothy T. Barrows,[1] Steve Juggins,[2] Patrick De Deckker,[3] Eva Calvo,[4] and Carles Pelejero[5]

Received 31 May 2006; revised 18 October 2006; accepted 6 December 2006; published 24 May 2007.

[1] We compile and compare data for the last 150,000 years from four deep-sea cores in the midlatitude zone of the Southern Hemisphere. We recalculate sea surface temperature estimates derived from foraminifera and compare these with estimates derived from alkenones and magnesium/calcium ratios in foraminiferal carbonate and with accompanying sedimentological and pollen records on a common absolute timescale. Using a stack of the highest-resolution records, we find that first-order climate change occurs in concert with changes in insolation in the Northern Hemisphere. Glacier extent and inferred vegetation changes in Australia and New Zealand vary in tandem with sea surface temperatures, signifying close links between oceanic and terrestrial temperature. In the Southern Ocean, rapid temperature change of the order of 6°C occurs within a few centuries and appears to have played an important role in midlatitude climate change. Sea surface temperature changes over longer periods closely match proxy temperature records from Antarctic ice cores. Warm events correlate with Antarctic events A1–A4 and appear to occur just before Dansgaard-Oeschger events 8, 12, 14, and 17 in Greenland.

Citation: Barrows, T. T., S. Juggins, P. De Deckker, E. Calvo, and C. Pelejero (2007), Long-term sea surface temperature and climate change in the Australian–New Zealand region, *Paleoceanography*, *22*, PA2215, doi:10.1029/2006PA001328.

1. Introduction

[2] Surface temperature is a direct expression of the energy balance of the Earth, which powers weather and surface circulation, and ultimately defines climate. Long and accurate records of surface temperature are vital to the study of climate change for a number of reasons. First, they allow us to assess the variability of climate change. This is clearest over the full amplitude of the most recent glacial-interglacial cycle. Second, they reveal the sensitivity of an area to climate change. This can be measured as the magnitude of temperature change from a full glaciation to an interglacial and is useful for identifying a region responsible for amplifying climate change. Third, the pattern of temperature change at a site can be compared directly to patterns expected from climate forcing mechanisms, revealing any relationships between the two. Last, the relative phasing of temperature versus forcing mechanisms reveals the response time of climate change.

[3] Deep-sea sediments provide the best archive of continuous high-quality temperature records outside the ice sheets. Climate at the sea surface is more spatially homogenous than in terrestrial environments and therefore changes recorded on the ocean floor can be representative of a wide region. A growing body of work in the Indian Ocean [e.g., *Williams*, 1976; *Howard and Prell*, 1992; *Wells and Wells*, 1994; *Labeyrie et al.*, 1996; *Martinez et al.*, 1999; *Mashiotta et al.*, 1999] and Pacific Ocean [e.g., *Wells and Okada*, 1997; *Weaver et al.*, 1998; *Sikes et al.*, 2002; *Pahnke et al.*, 2003] describes sea surface temperature (SST) changes over the last glacial cycle, mostly employing planktonic foraminifera. However, most of these records lack the temporal resolution required to identify millennial-scale fluctuations, or the faunal SST methods used have large uncertainty [*Barrows et al.*, 2000]. Additionally, a variety of age models have been used making it difficult to compare the timing of climate events between records.

[4] Long, high-quality surface temperature records for the Pleistocene of continental Australia and New Zealand are comparatively rare. This is principally due to a lack of suitable geological proxies for temperature preserved in a continuous recording medium. Although the formation of cold climate landforms (i.e., glacial and periglacial) is strongly related to temperature change, glaciation of Australia was limited and brief. Recent advances in the direct dating of these cold climate landforms [*Barrows et al.*, 2002, 2004] have improved the glacial stratigraphy. Glaciation of nearby New Zealand was more extensive, and the availability of carbonaceous material in glacial deposits has allowed more chronological control [*Suggate and Almond*, 2005]. However, the degree to which temperature change alone was

[1]Department of Nuclear Physics, Australian National University, Canberra, ACT, Australia.
[2]School of Geography, Politics and Sociology, University of Newcastle, Newcastle upon Tyne, UK.
[3]Department of Earth and Marine Sciences, Australian National University, Canberra, ACT, Australia.
[4]Institut de Ciències del Mar, Consejo Superior de Investigaciones Cientificas, Barcelona, Spain.
[5]Institució Catalana de Recerca i Estudis Avançats and Institut de Ciències del Mar, Consejo Superior de Investigaciones Cientificas, Barcelona, Spain.

0883-8305/07/2006PA001328$12.00

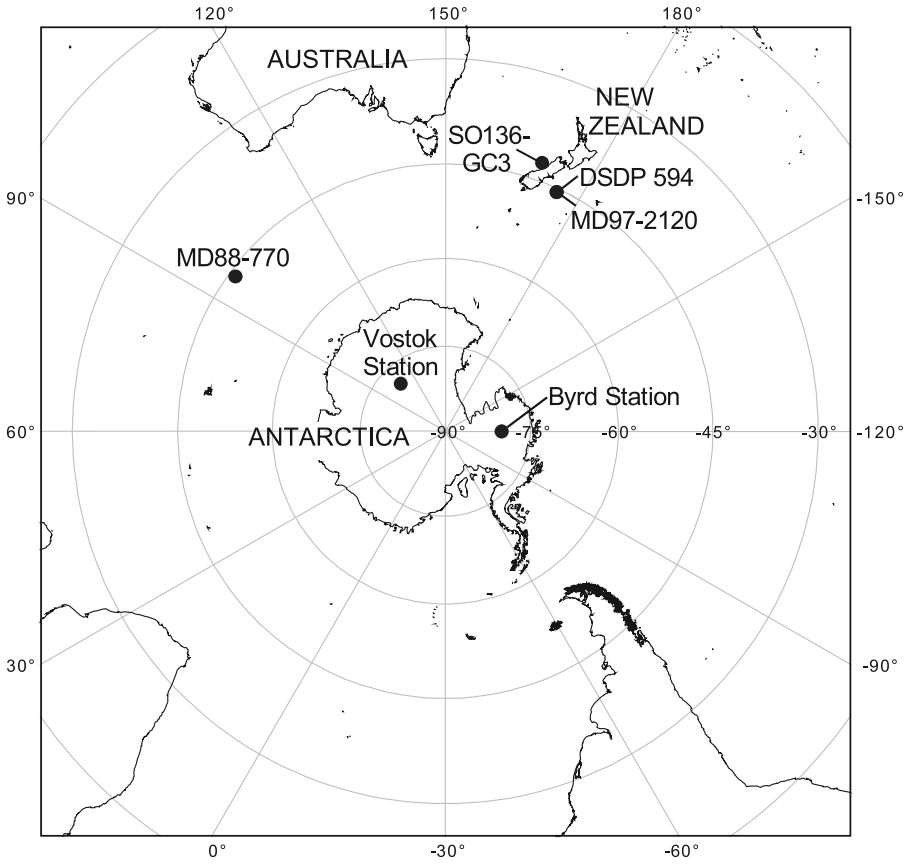

Figure 1. Regional map showing core sites and sites mentioned in the text.

responsible for driving glacier advances on either side of the Tasman Sea during the Late Pleistocene is uncertain. Similarly, terrestrial pollen records are very difficult to date beyond the radiocarbon timescale [e.g., *Vandergoes et al.*, 2005] and the extent to which they reflect temperature changes is low [*Kershaw et al.*, 2004]. Well-dated, accurate records of temperature change from the adjacent oceans are therefore essential for comparing with these records to better understand patterns of climate change.

[5] In this paper, we present a new 150,000-year temperature record derived from core SO136-GC3 in the Tasman Sea and reevaluate long records of SST change from three other sites adjacent to southern Australia and New Zealand. Sea surface temperature estimates are based on planktonic foraminifera assemblages using state-of-the-art approaches. Combined with a new independent record of SST provided by the $U^{K'}_{37}$ index on the same core [*Pelejero et al.*, 2006] we make comparisons with records from the highest-resolution cores in the region (MD88-770, MD97-2120 and DSDP site 594). We determine the timing of major SST changes relative to other proxies of climate change in these cores, especially terrestrial sediment influx and pollen, by placing all records onto a common timescale. We look at the pattern of climate change in the midlatitudes of the Southern Hemisphere over the last glacial cycle to examine likely causes and to assess whether the response is more similar to the Antarctic or Greenland pattern of climate change [*Alley and Clark*, 1999].

2. Methods

2.1. Cores

[6] Core SO136-GC3 was collected during a RV SONNE cruise on the Challenger Plateau (42°18′S, 169°53′E, water depth 958 m) in 1998 (Figure 1). The core consists of green-grey fine silt rich in planktonic foraminifera. The top 5 cm of sediment were too unconsolidated for recovery. Bioturbation was observed in the form of burrows (probably by echinoderms) in some parts of the core but no turbidites were recorded during logging [*Thiede and Nees*, 1999]. Samples of sediment between 3 and 6 cm^3 were taken from contiguous 2-cm-thick slices along the length of the core. For radiocarbon dating, oxygen isotope analysis and planktonic foraminifera counting, the sediment was disassociated in 3% hydrogen peroxide, washed through a 100 μm sieve, and the coarse fraction retained.

[7] For comparison with SO136-GC3, we chose three other midlatitude cores in the Australasian sector of the Southern Ocean: MD88-770 (46°01′S, 96°27′E, 3290 m) from the Indian Ocean [*Bareille et al.*, 1994; *Labeyrie et al.*, 1996], and DSDP site 594 (45°31.41′S, 174°56.88′E, 1204 m) and MD97-2120 (45°32.06′S, 174°55.85′E, 1210 m) both from east of New Zealand [*Nelson et al.*,

1994; *Pahnke et al.*, 2003; *Pahnke and Zahn*, 2005] (Figure 1). These cores were selected on the basis of their relatively high resolution, the quality of the data, and the presence of pollen data and sediment analyses.

2.2. Planktonic Foraminifera and Sea Surface Temperature

[8] For SO136-GC3, planktonic foraminifera were counted in the >150 μm fraction, which was subsampled using a microsplitter. Counts were performed on every level down to 2 m, after which about 2 out of every 3 samples were counted, focusing on major faunal transitions. We aimed to identify at least 400 specimens to minimize counting errors, following the taxonomy of *Saito et al.* [1981] modified by *Kennett and Srinivasan* [1983], *Hemleben et al.* [1989], and *Chapronière* [1991].

[9] For MD88-770, we use the published foraminifera counts of *Labeyrie et al.* [1996] and for DSDP site 594 we combine the counts from *Wells and Okada* [1997] and *Weaver et al.* [1998]. To remove methodological bias, we recalculate SST from all cores using the same approach. Estimates are made using the modern analog technique (MAT), the revised analog method (RAM) [*Waelbroeck et al.*, 1998] and artificial neural networks (ANN) in conjunction with the AUSMAT-F4 database [*Barrows and Juggins*, 2005]. This database uses only Southern Hemisphere data because of faunal endemism. Such an approach gives better performance than smaller regional databases [*Barrows et al.*, 2000]. Results from the three techniques are averaged to make a consensus prediction, providing the best available approach using planktonic foraminifera for the Southern Hemisphere [*Barrows and Juggins*, 2005]. Under fivefold leave-out cross-validation, the root mean square error of prediction (RMSEP) for the "consensus" faunal estimates is ±0.77°C, although this figure is likely to be overly optimistic because of spatial dependence in the training and validation data sets [*Telford and Birks*, 2005]. We assessed the quality of the SST estimates following the same approach as *Barrows and Juggins* [2005].

[10] We compare the three faunal SST records with results from two biogeochemical techniques; a new alkenone SST record from SO136-GC3 [*Pelejero et al.*, 2003, 2006] and the Mg/Ca SST record from MD97-2120 of *Pahnke et al.* [2003]. Full details for the alkenone analyses are given by *Pelejero et al.* [2006]. To derive SST estimates, these authors use the global equation of *Müller et al.* [1998]. The standard error of regression for this equation is ±1.5°C. This error is larger than that reported by *Prahl et al.* [1988] for a laboratory environment (±0.6°C) and reflects additional uncertainties from making measurements on marine sediment in multiple independent laboratories. The SST estimates used here from *Pahnke et al.* [2003] are derived from the calibration of *Mashiotta et al.* [1999], which has a standard error of ±1.1°C. The calibration used cultured specimens down to 16°C (the maximum SST estimated in MD97-2120) and was extended down to 10°C by including two subantarctic core tops. Estimates below 10°C (about half the estimates in MD97-2120), are beyond the calibration limits, and so the error is difficult to judge. The systematic offset at the maximum and minimum Mg/Ca values in MD97-2120 between the calibration of *Mashiotta et al.* [1999] and that of *Elderfield and Ganssen* [2000] equates to SST differences of 0.2°C and 0.5°C respectively.

[11] Different proxies are subject to different sources of errors. Although the error for both biogeochemical techniques is greater than that of the faunal estimates, these techniques have the advantage of higher measurement precision than faunal assemblages, resulting in less "noisy" reconstructions. Because of the need to produce a calibration curve, both $U^{K'}_{37}$ and Mg/Ca are more prone to systematic errors than the faunal estimates, which are not based on single equations. When different calibrations are used, this results in a systematic displacement between the estimates. In all cases, the first-order temperature change between glacial and interglacial periods is the most reliable for interpretation, but because of the inherent errors, we will only focus in SST fluctuations larger than 1.5°C.

2.3. Stable Isotope Stratigraphy

[12] Stable isotope analyses for SO136-GC3 were conducted on the planktonic foraminifera *Globigerina bulloides*. Approximately 200 μg of foraminifera were picked from the >150 μm fraction, cleaned with alcohol in an ultrasonic bath, and rinsed twice in distilled water. Measurements were conducted on a Finnigin-MAT251 mass spectrometer with a carbonate Kiel device at the Research School of Earth Sciences, The Australian National University. Oxygen and carbon stable isotope data are reported in δ notation relative to the V-PDB standard. Samples were run against the NBS-19 calcite standard using values of $\delta^{13}C_{V\text{-}PDB}$ = +1.95 ‰ and $\delta^{18}O_{V\text{-}PDB}$ = −2.20‰ for calibration of the working gas. External precision of the measurements on the standard (N = 133) was ±0.02 ‰ and ±0.03 ‰ for δ^{13}C and δ^{18}O respectively. The internal precision of sample measurements was always better than 0.03‰ for δ^{13}C and 0.07‰ for δ^{18}O. Twenty-seven samples were run in duplicate and one sample in triplicate. The external error on sample duplicates was ±0.17‰ (0.01–0.69‰) and ±0.20 ‰ (0–0.68‰) for δ^{13}C and δ^{18}O respectively. This scatter is an order of magnitude higher than expected, indicating sample heterogeneity. Typically 5 to 20 specimens were needed to ensure 200 μg. It appears that this number of individuals is insufficient to integrate seasonal changes, and mixture because of bioturbation within the sampled horizons.

[13] For the oxygen isotope (δ^{18}O) stratigraphy of the other three cores, we use benthonic foraminiferal records where available. For DSDP site 594, we use the benthonic foraminifera (mostly *Uvigerina* sp.) and *Gg. bulloides* δ^{18}O records of [*Nelson et al.*, 1993]. The δ^{18}O record of MD88-770 [*Labeyrie et al.*, 1996] is a composite made from the following three benthonic species adjusted for "vital effects": *Cibicidoides wuellerstorfi* (+0.64‰), *Melonis barleeanum* (+0.40‰), and *Epistominella exigua* (+0.22‰). Finally, for MD97-2120, we use the high-resolution planktonic foraminiferal (*Gg. bulloides*) δ^{18}O record and the composite benthonic δ^{18}O record derived from *Cibicidoides* spp. and *M. barleeanum*, both adjusted by +0.64‰ [*Pahnke et al.*, 2003].

Table 1. Radiocarbon Dates for SO136-GC3

Lab Identification	Interval, cm	Date, ^{14}C years B.P.	δ^{13}C, ‰	Age, cal years B.P.	Plus, years	Minus, years	68% CI[a]
KIA-15517	5–6	3,860 ± 35	−3.59 ± 0.21	3,830	100	70	3,730–3,900
KIA-14358	10–12	6,440 ± 45	−2.36 ± 0.12	6,930	120	90	6,810–7,020
KIA-15518	14–16	6,755 ± 40	−1.63 ± 0.10	7,290	50	70	7,240–7,360
KIA-15519	18–20	11,500 ± 60	−1.45 ± 0.09	13,020	100	130	12,920–13,150
KIA-14359	22–24	12,250 ± 70	−1.87 ± 0.14	13,690	200	330	13,490–14,020
KIA-14360	30–32	15,760 ± 90	+0.12 ± 0.17	18,260	300	290	17,960–18,550
KIA-14361	38–40	17,460 ± 100	+2.14 ± 0.08	20,210	340	340	19,870–20,550
KIA-14362	48–50	18,870 ± 110	+2.20 ± 0.18	21,840	370	360	21,470–22,200
NZA-11004	52–54	19,720 ± 150	+0.04	22,990	340	260	22,650–23,250
KIA-14363	70–72	22,470 +190/−180	+2.25 ± 0.21	26,800	430	430	26,370–27,230
KIA-14364	76–78	23,770 +190/−180	−1.91 ± 0.27	28,430	380	390	28,050–28,820
KIA-15520	94–96	28,710 +350/−340	−1.72 ± 0.04	33,140	810	810	32,330–33,950
KIA-15521	108–110	29,820 +360/−350	−1.62 ± 0.10	34,770	500	500	34,270–35,270
KIA-15522	120–122	32,570 +510/−480	−0.54 ± 0.11	37,660	790	800	36,870–38,460
KIA-15523	132–134	43,990 +2170/−1710	−2.51 ± 0.21	46,600	2040	2030	44,560–48,630

[a]CI is confidence interval.

2.4. Radiocarbon Dating and Calibration

[14] Radiocarbon dating of SO136-GC3 was performed on *Gg. bulloides*. Fourteen samples of at least 8 mg were picked from the >150 μm fraction. The samples were cleaned with 15% H_2O_2 in an ultrasonic bath to remove fine particles and analyzed by accelerator mass spectrometry at Kiel University, Germany. A single additional radiocarbon date (NZA-11004) is also available from G. van der Lingen (personal communication, 2004) (Table 1).

[15] Radiocarbon dates are available for each of the other three cores. For MD88-770, there are 18 dates on specimens of *Neogloboquadrina pachyderma* (left coiling) [*Labeyrie et al.*, 1996]. There are nine radiocarbon dates on *Gg. bulloides* for MD97-2120 down to 267 cm. Between 267 cm and 634 cm, six dates are available on combined samples of *Gg. bulloides* and *N. pachyderma*. Only four radiocarbon dates are available for DSDP site 594 [*Black et al.*, 1988; *Wells and Okada*, 1997] on samples of *Gg. bulloides*.

[16] Radiocarbon dates up to 22,850 cal years B.P. are calibrated using the INTCAL98 marine curve in conjunction with CALIB 4.4 [*Stuiver et al.*, 1998]. Older dates are calibrated using the CALPAL 2004 SFCP calibration curve and the University of Cologne Radiocarbon Calibration Program Package (CALPAL). Radiocarbon dates are expressed in radiocarbon years (^{14}C years B.P.) and calibrated radiocarbon dates are expressed as calibrated years (cal years B.P.).

[17] Reservoir corrections are estimated using the CALIB Marine Reservoir Correction Database. A ΔR value for regional New Zealand of −11 ± 50 (or 275 ± 50 years) is used for SO136-GC3, DSDP Site 594 and MD97-2120 but for *Gg. bulloides* it should be considered a minimum given that this species can live and calcify deeper than 100 m. For MD88-770 we use a regional South Australia average of ΔR = 61 ± 50 (or 350 ± 50 years). For the Southern Ocean, this is likely to be an underestimate by at least 350 years during glacial intervals because of frontal movements [*Bard*, 1988], but this correction is not well constrained.

3. Age Models

[18] To enable comparisons between the four cores studied here, we standardized the stratigraphy of each core by constructing new age models using a single consistent approach. For the uppermost part of each core, we use available ^{14}C ages as tie points. Below this, we pattern match δ^{18}O records against the benthonic oxygen isotope chronostratigraphy of MD95-2042 on the GISP timescale [*Shackleton et al.*, 2004]. We prefer this target stratigraphy to the chronology of *Martinson et al.* [1987] on the SPECMAP benthonic stack [*Pisias et al.*, 1984], because it is a more precise and higher-resolution chronology against which to assess millennial-scale variability, and it does not rely on any assumptions related to orbital forcing.

[19] To increase the robustness of the fit with the target chronostratigraphy, we apply a three-point running mean to each of the δ^{18}O records (except the lower-resolution benthonic δ^{18}O record of MD88-770) to integrate high-amplitude, high-frequency variability that is probably small sample noise, as seen in SO136-GC3. Where possible, we use the event stratigraphy of *Prell et al.* [1986] for tie points; elsewhere, we matched to prominent peaks and troughs. Age tie points for each core are listed in the auxiliary material.[1] See also the Australian Quaternary Data Archive at http://www.aqua.org.au/archive.html.

[20] Pattern matching is only valid if there is no systematic age offset between the two recording mechanisms. *Skinner and Shackleton* [2005] determined a 4000-year offset between equatorial Pacific and North Atlantic Ocean benthonic δ^{18}O records. This is larger than both the previous observation by *Duplessy et al.* [1991] during deglaciation and the lag observed by *Barrows et al.* [2000] in the southwest Pacific Ocean. We expect some displacement between the planktonic and benthic δ^{18}O records compared here because of SST and water mass age differences. The mixing time of the deep ocean sets a systematic limit on the accuracy of the correlation between oxygen isotope events between the North Atlantic and the cores used here. This is currently about 1000 years in the Southern Ocean [*Matsumoto and Key*, 2004], and is a minimum for the LGM and other glacial periods, but was probably similar during warm periods in the past.

[1]Auxiliary materials are available at http://www.ncdc.noaa.gov/paleo/paleo.html.

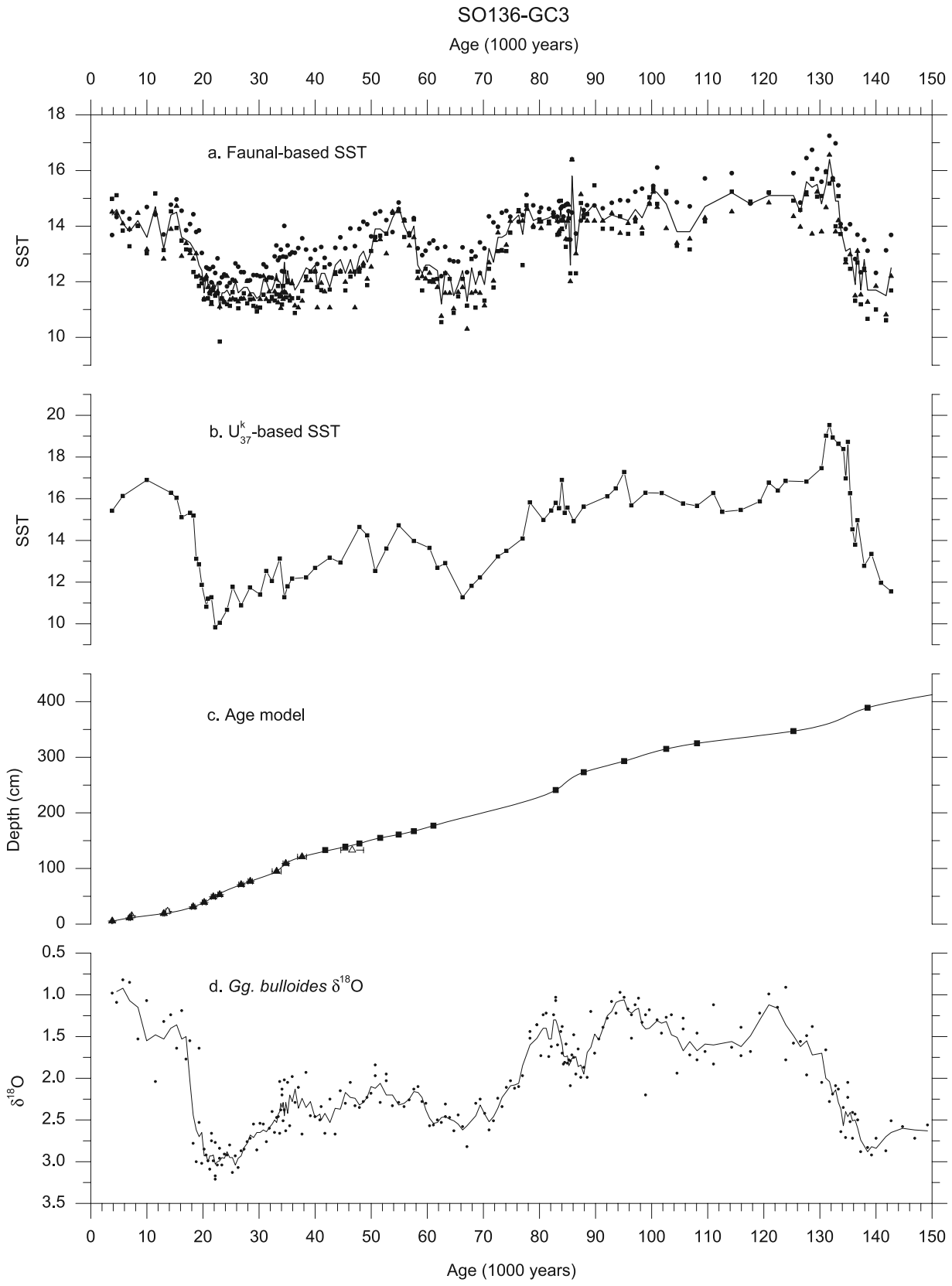
SO136-GC3
Age (1000 years)
a. Faunal-based SST
SST
b. U^{k}_{37}-based SST
c. Age model
Depth (cm)
d. *Gg. bulloides* $\delta^{18}O$
$\delta^{18}O$

Figure 2

[21] Each age model was constructed using a basic spline fit through age tie points with no smoothing. This model produces more realistic sedimentation rate changes than linear interpolation. Radiocarbon ages were filtered on quality and consistency. We only use ages up to 38,000 years because of the uncertainty of calibration and this is usually the point where the first reliable oxygen isotope events may be identified. Consequently, the period 22,000–39,000 years does not have strong age control in all cores. Dates excluded from the age models are displaced on the age curve suggesting contamination by younger carbon. In all cases, the exclusion of these dates significantly improves the fit of the age depth curve.

[22] Sedimentation rates vary by up to an order of magnitude within each core. SO136-GC3 has the lowest sedimentation rates, from only 1–13 cm 1000 yr^{-1}. Samples integrate sediment deposited over 200 to 4000 years. The other three cores have sedimentation rates varying from 3 to 50 cm 1000 yr^{-1}. The core with the highest sample resolution is MD88-770, where each sample represents 100–3000 years. Sedimentation rates are generally lowest during the Holocene and interglacial periods and highest during glacial periods and terminations.

[23] On the basis of the sampling intervals, errors on the radiocarbon dates, errors in the fitting procedure, and the use of planktonic $\delta^{18}O$ for two cores, the errors in the age models probably range from 200–1000 years in the youngest radiocarbon-dated section (<22,000 years), 1000–3000 years from 22,000–90,000 years and up to 5000 years beyond this. The ages may be systematically too old if the reservoir effect has been underestimated during glacial periods.

4. Results

4.1. Sea Surface Temperature Estimates

[24] The quality of the new faunal SST estimates is high. The squared chord "distance" between fossil and modern samples provides a good measure of how well the training set provides analogs for the down-core assemblages [*Barrows and Juggins*, 2005]. The average is below 0.1 for all cores (SO136-GC3, 0.058; DSDP site 594, 0.045; MD88-770, 0.024). The greatest distances (SO136-GC3, 0.126; DSDP site 594, 0.143; MD88-770, 0.078) are found during interstadial periods, namely the warm periods in oxygen isotope chronozones (OIC) 3 and 5. Conversely, the best matches with the lowest distances are found during the glacial periods, particularly OIC 2. These differences are related to species diversity; the most diverse faunas are found in warmer water, so analogs are harder to find and so distances tend to be greater. A higher density of core tops is required in the temperate zone to capture the full faunal diversity compared to the relatively simple fauna in the subantarctic. This phenomenon is also reflected in the variability between the analogs as measured by the standard deviation between the top four analogs selected by the MAT. The lowest average standard deviation is given by MD88-770 (0.7°C), followed by DSDP site 594 (0.9°C) and SO136-GC3 (1.1°C).

[25] A measure of methodological consistency is given by the standard deviation between the three SST estimation methods. Typically, the two analog methods provide similar results, but in several cases, particularly in the warmer sections of SO136-GC3 and DSDP site 594, the two methodologies diverge. In SO136-GC3, ANN produces systematically warmer estimates. Therefore this core has the highest methodological standard deviation (0.7°C), followed by DSDP site 594 (0.6°C), and MD88-770 (0.4°C). Consequently, the southernmost core MD88-770 provides the most consistent faunal SST estimates, followed by DSDP site 594 and SO136-GC3.

[26] The alkenone SST estimates for SO136-GC3 provide an independent estimate of temperature change for this core. Despite being an entirely different method of SST reconstruction, the pattern of change between the two records is clearly similar (Figure 2). The main difference between the two records (considering the errors) is that the overall amplitude of the $U^{K'}_{37}$-SST estimates is greater; being up to 3°C warmer during interglacial periods and up to 1°C colder during the LGM. In addition, there are more subtle differences between the two sets of estimates in regard to some of the finer-scale structure of SST change, particularly in OIC3 and 5. There is no simple explanation for these technique-specific differences. Faunal SST estimates are inherently more "noisy" because of the presence of variables other than temperature that influence faunal assemblage composition. On the other hand, alkenones are more prone to lateral transport/reworking, and the SST estimates are vulnerable to variability in the seasonal timing of maximum productivity of haptophyte algae.

4.2. Patterns and Timing of Temperature Change

[27] New SST estimates for SO136-GC3, DSDP site 594 and MD88-770 are plotted in Figures 2–4, together with existing estimates for SO136-GC3 [*Pelejero et al.*, 2003, 2006] and MD97-2120 (Figure 5) [*Pahnke et al.*, 2003]. There are clear similarities between the SST records in the first-order pattern of change over the last glacial cycle. A notable trend among the records is that the greatest response to climate change is in the Southern Ocean, on both orbital and suborbital timescales. This sensitivity is expressed both in the greatest magnitude of SST change over the glacial-interglacial cycle and by the amount of variability in the record. The least sensitive record is that of SO136-GC3 in the Tasman Sea. Temperature records in cores from further north show even less variability [*Lea et al.*, 2000; *Martinez*

Figure 2. SO136-GC3: (a) Consensus estimates of SST from planktonic foraminifera (squares indicate the modern analog technique (MAT), triangles indicate the revised analog method (RAM), and circles indicate the artificial neural networks (ANN). (b) SST record from the $U^{K'}_{37}$ index [*Pelejero et al.*, 2006]. (c) Age model (triangles indicate radiocarbon dates with 1 σ error bars, and squares indicate oxygen isotope age tie points). Solid symbols were used to construct the age model. (d) Oxygen isotope record for *Gg. bulloides*. The line represents a three-point running mean.

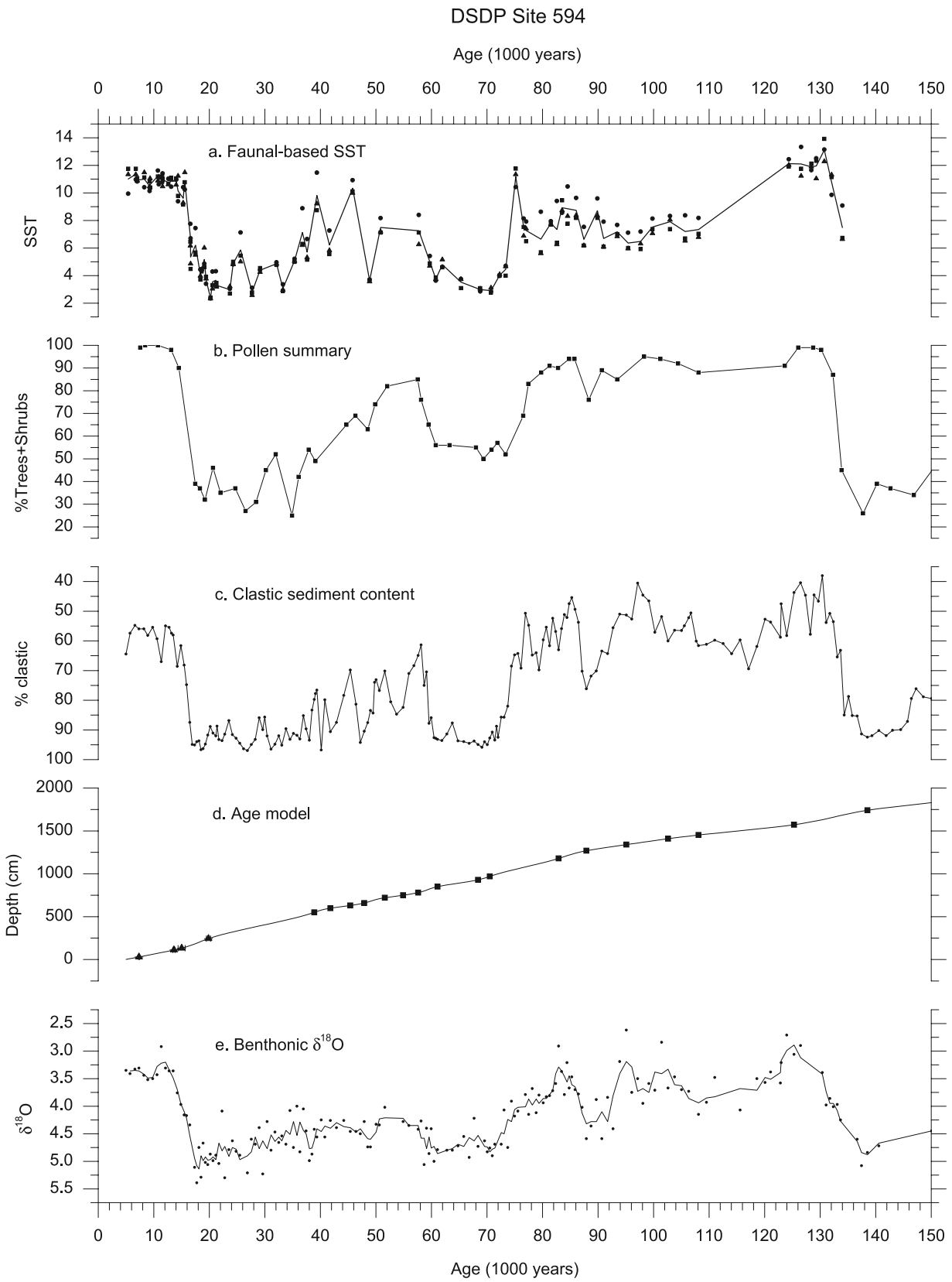
DSDP Site 594
Age (1000 years)
a. Faunal-based SST
SST
b. Pollen summary
%Trees+Shrubs
c. Clastic sediment content
% clastic
d. Age model
Depth (cm)
e. Benthonic δ18O
δ18O
Age (1000 years)

Figure 3

et al., 2002]. The most sensitive record is that of MD88-770, and similar features are present in other cores nearby [*Hays et al.*, 1977; *Mashiotta et al.*, 1999]. Both DSDP site 594 and MD97-2120 east of New Zealand near the subantarctic interface of the subtropical front display features intermediate between those extremes.

[28] In all records, OIC 6, 4, and 2 are periods of maximum cold exhibiting little difference in magnitude of cooling. The onset of strong cooling during the best-characterized glacial period (OIC 2) has variable timing between the five records. In general, the cores in the coldest water are first to experience maximum cooling.

[29] The character of interglacial OIC 5 varies considerably between the various SST records. All five records show maximum SST during 5e, the warmest period for the last 150,000 years. The most structure is visible in DSDP Site 594 and MD97-2120 and especially MD88-770, where the SST shows great variability beyond the analytical error, plunging to near glacial maximum temperatures during 5b and 5d, and increasing to near Holocene temperatures during 5c and 5e (Figure 4).

[30] Similar to OIC 5, the structure of interstadial OIC 3 varies considerably between the five SST records. In most records, warmest SST occurs early in the chronozone, and then secular cooling follows, with peaks in SST generally successively cooler.

[31] The transition to the Holocene is characterized by rapid warming immediately after the LGM in all records. Temperature increase during the interval from 20 cal years B.P. until ~15 cal years B.P. accounts for most of the postglacial warming. The highest-resolution record of MD88-770 is characterized by a brief rapid oscillation in SST at the beginning of deglaciation, followed by two lesser magnitude events. The oscillation occurs shortly after the LGM, at 19.4 cal years B.P. when there is warming of 5°C in only ~130 years. This is the most rapid, highest-magnitude warming in the record. Similar rates of warming occur in OIC 5, where warming of 5.9°C after the penultimate deglaciation occurs in only ~190 years, and in OIC 3. After 19.2 cal years B.P. cooling is almost as rapid and SST returns to near glacial maximum conditions at 18.5 cal years B.P. Similar, but lower magnitude, cooling occurs after warm events during OIC 3, so rapid cooling is not unique in this record. Although this event is well beyond the analytical errors of the SST estimates, it takes place over only a few samples, so its representativeness is difficult to assess. In MD97-2120 [*Pahnke et al.*, 2003], there is a brief cold reversal at 17.8 cal years B.P., which is likely to represent the same event given likely age model errors. The event also has a likely counterpart in the radiolarian SST record of RC11-120 [*Morley*, 1989]. This event is not seen in other nearby records [e.g., *Mashiotta et al.*, 1999], which is perhaps unsurprising given these are more coarsely sampled.

5. Discussion

5.1. Terrestrial Correlations

5.1.1. Proxy Glaciation Records

[32] The longest continuous record in the Australasian sector of the Southern Ocean that can be related to ice advance and retreat is the clastic content/carbonate content in DSDP site 594 [*Nelson et al.*, 1993]. This record relates to ice extent on the South Island of New Zealand, one of the largest glaciated zones in the midlatitude Southern Hemisphere. By placing DSDP site 594 on the common timescale with the other cores, we can directly compare glacier fluctuations with the higher-resolution SST records to evaluate the degree to which glacier extent is explained by SST variations representative of the midlatitudes.

[33] The first-order features of the clastic record mirror the SST variations (Figure 3). Maxima in clastic content coincide with known well-dated glacier advances in Australia and New Zealand [*Barrows et al.*, 2001, 2002; *Suggate*, 1990; *Suggate and Almond*, 2005]. The close relationship between dated moraines, the clastic record and SST supports temperature as being the major controlling variable in glaciation.

[34] Clastic levels indicate that the extent of glaciation was similar in OIC 6, 4, and 2 and more restricted glaciation occurred in OIC 5e than during the Holocene (Figure 3). The clastic content during OIC 3 resembles the higher-resolution SST records, particularly that of MD88-770. There are four distinct minima at 58, 52, 45 and 39 ka, at the same time as the SST peaks. A key feature of OIC3 is the rapid change in the flux of clastic material to the core site. If interpreted simply, glaciers advanced and retreated rapidly in synchrony with SST changes. There is an asymmetry between the rate of retreat (decreasing clastic content) and the rate of advance of ice (increasing clastic content) given the same ''extents,'' the latter taking about twice as long. A similar phenomenon is observed in the SST records where warming occurs up to five times quicker than cooling. This indicates rapid response time by mountain glaciation.

[35] Clastic content decreases rapidly after 17 ka, reaching Holocene levels by 14.9 ka (Figure 3). This rapid deglaciation is consistent with the SST increase after the LGM, which is largely complete by 15 ka. Basal ^{14}C dates from Blue Lake, New South Wales, and lakes in Tasmania [*Barrows et al.*, 2002] confirm rapid deglaciation in Australia at the same time.

[36] There is a significant clastic maximum at 18.5 ka (Figure 3), which occurs at a similar time to the last significant glacier advance of OIC 2 in New Zealand and Australia [*Suggate and Almond*, 2005]. Its timing is

Figure 3. DSDP site 594: (a) Consensus estimates of SST from planktonic foraminifera (squares indicate MAT, triangles indicate RAM, and circles indicate ANN). (b) Percentage of trees and shrubs in pollen data. The line represents a spline fit through the data of *Heusser and Van de Geer* [1994]. (c) Percentage of clastic content in sedimentary record [*Nelson et al.*, 1993]. (d) Age model (triangles indicate radiocarbon dates with 1 σ error bars, and squares indicate oxygen isotope age tie points). Radiocarbon dates are from *Black et al.* [1988] and *Wells and Okada* [1997]. (e) Oxygen isotope record for *Uvigerina* sp. [*Nelson et al.*, 1993]. The line represents a three-point running mean.

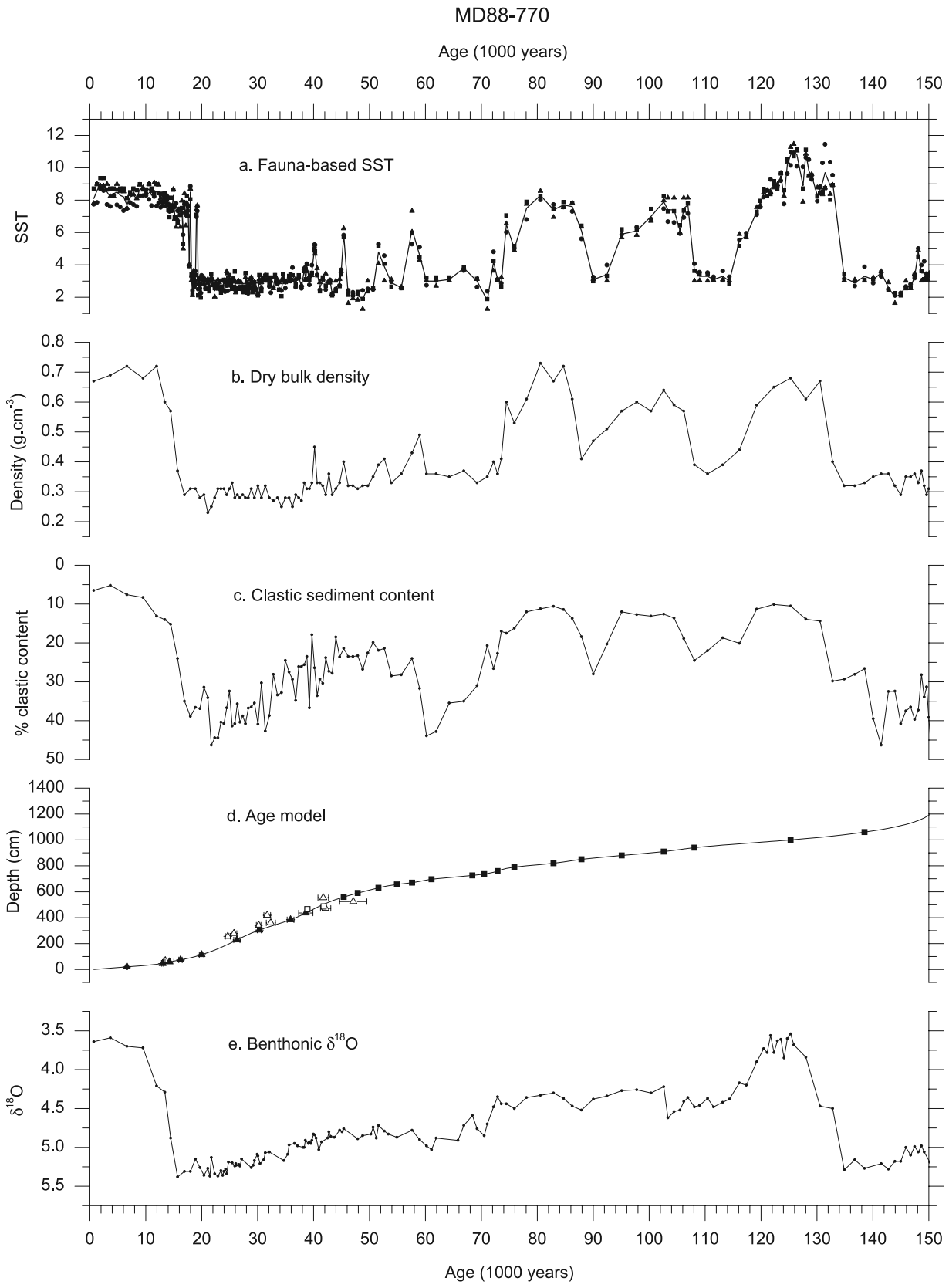
MD88-770
Age (1000 years)
a. Fauna-based SST
SST
b. Dry bulk density
Density (g.cm-3)
c. Clastic sediment content
% clastic content
d. Age model
Depth (cm)
e. Benthonic δ18O
δ18O
Age (1000 years)

Figure 4

also very similar to the rapid cold reversal at 18.5 ka in MD88-770. Therefore it is possible that abrupt cooling soon after the LGM was responsible for the final major ice advance of glaciers during OIC 2 on both sides of the Tasman Sea, but the dating of the advance is not definitive.

[37] The clastic content in core MD88-770 is plotted in Figure 4 and represents a number of contributions of detrital material into the Southern Ocean resulting from a variety of sources (as opposed to DSDP site 594) including glaciers, the continental shelves, and ice-rafted debris from Antarctica [*Bareille et al.*, 1994]. The pattern of change of clastic content in MD88-770 bears first-order similarities to the SST record from the same core, with the important difference that the magnitude of the changes within the interstadial periods (during OIC 5 and 3) are not as great. There are five decreases in clastic content during OIC 3 at 58, 51, 44, 40 and 35 ka that correspond to SST increases, and also to clastic content decreases in DSDP site 594. Clearly SST is linked closely to the mechanisms producing and transporting the clastic material to this region to the Southern Ocean, probably through glacier/ice sheet fluctuations.

[38] The dry bulk density of the sediment in MD88-770 [*Bareille et al.*, 1994] is also shown in Figure 4. Bulk density halves during glacial periods as opposed to interglacial periods, dominantly reflecting the replacement of carbonate ooze (dominated by foraminifera) by siliceous ooze (dominated by diatoms). This change occurs primarily as a response to surface cooling, and so it is unsurprising that there is a strong resemblance to the SST record from the same core. Variations in density occur with a very similar pattern, both in timing and magnitude to variations in temperature.

[39] Finally, lightness (L*) measurements from MD97-2120 [*Michel and Turon*, 2006] are shown in Figure 5c. Lightness of deep-sea sediment is usually a function of inorganic content (such as clastic content) and biogenic carbonate (such as foraminifera) versus organic matter content (which is usually darker). The resemblance to the nearby clastic content record of DSDP site 594 is striking and suggests a similar provenance for the shape of the lightness record. To some extent, lightness must also record surface productivity changes. This is illustrated by comparison with the alkenone concentration in the same sediment shown in Figure 5b [*Sachs and Anderson*, 2005]. Increases in algal productivity occur at about the same time as warming events.

5.1.2. Proxy Vegetation Record

[40] The pollen record from DSDP site 594 [*Heusser and Van de Geer*, 1994] is presented in Figure 3. The proportion of tree and shrub pollen indicates the relative dominance of vegetation types on nearby New Zealand through time, which in turn reflects changing terrestrial climate, mainly precipitation and temperature. There are few age constraints on terrestrial pollen records beyond the range of radiocarbon [e.g., *Vandergoes et al.*, 2005]. Placing the pollen record on the Greenland chronology using the age model for DSDP site 594, we can directly compare vegetation changes with SST records on an absolute timescale.

[41] The pollen record shares a number of features with the SST and clastic content records from the same core with similar timing for all major changes. Overall, 51% of the variance in the proportion of tree and shrub pollen can be accounted for by the SST estimates (and by variables that simply correlate with temperature). Although only accounting for half the variance, SST is clearly closely linked with land surface climate. Tree/shrub pollen decreases in abundance during OIC 4, but not to the levels of OIC 6 or 2. Temperature during OIC4 was similar to that of the glacial maxima, so this may indicate that OIC 4 was relatively wetter than other glacial periods with less environmental stress on trees. The sampling resolution during OIC 3 is not sufficient to test whether vegetation responded to the observed SST fluctuations during this period, but from comparison with the Okarito Pakihi record of *Vandergoes et al.* [2005], this looks likely. The correspondence between pollen changes and the SST record, especially during the rapid transitions from OIC 5 to 4 and from OIC 2 to 1, indicates a rapid response time by major vegetation zones to climate change.

[42] The close similarities between glacial records, clastic input into the Southern Ocean and vegetation changes in New Zealand, demonstrate close links between terrestrial climate change and nearby SST. In particular, the four warming periods within OIC 3 appear to be pervasive features of a wide variety of midlatitude climate change records. The Southern Ocean appears to act as a sensible heat sink or source that synchronizes climate change in Australia and New Zealand.

5.2. Insolation Changes and Sea Surface Temperature

[43] Three independent SST estimation techniques and other independent proxies from four individual high-resolution cores presented on a common, accurate chronostratigraphy provides us with a robust basis from which to examine climate change on both orbital and millennial timescales in the Australia–New Zealand region. The currently accepted theory is that insolation change in the high latitudes of the Northern Hemisphere sets the rhythm of global climate change on the 10^4-year timescale [*Hays et al.*, 1977; *Imbrie et al.*, 1992]. We can provide a test as to whether this theory holds in the Australasian sector of the Southern Hemisphere by comparing the timing of major events in the proxy climate records with the midsummer insolation values at 65°N. To aid the comparison, we construct a Southern Ocean stacked SST record by averaging the two highest-resolution records, MD88-770 and MD97-2120. Stacking reduces dependency on both age models and the SST technique used in the individual cores.

[44] The timing of major temperature changes is consistent with orbital forcing of climate in the Northern Hemisphere (Figures 2–6). There are no clear systematic differences or

Figure 4. MD88-770: (a) Consensus estimates of SST from planktonic foraminifera (squares indicate MAT, triangles indicate RAM, and circles indicate ANN). (b) Dry bulk density of the sediment [*Bareille et al.*, 1994]. (c) Clastic sediment content (%) [*Bareille et al.*, 1994]. (d) Age model (triangles indicate radiocarbon dates with 1 σ error bars, and squares indicate oxygen isotope age tie points). Radiocarbon dates are from *Labeyrie et al.* [1996]. Solid symbols were used to construct the age model. (e) Composite benthonic oxygen isotope record [*Labeyrie et al.*, 1996].

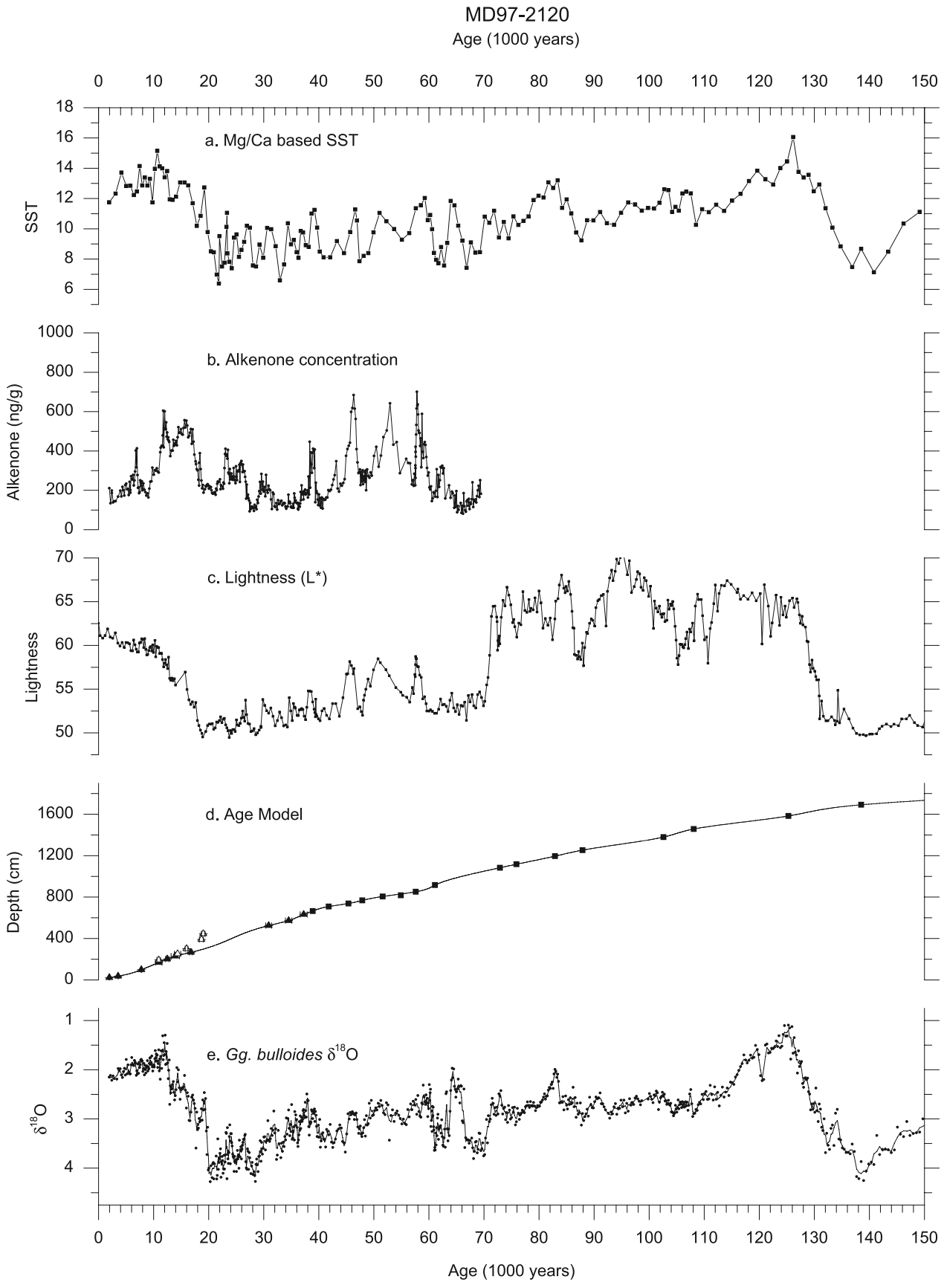
MD97-2120
Age (1000 years)
a. Mg/Ca based SST
SST
b. Alkenone concentration
Alkenone (ng/g)
c. Lightness (L*)
Lightness
d. Age Model
Depth (cm)
e. Gg. bulloides δ18O
δ18O
Age (1000 years)

Figure 5

geographic trends in the timing of SST events (maxima and minima) versus insolation maxima and minima within the uncertainty we expect in the chronologies (Figure 6). The best matches occur during the interglacials OIC 5 and OIC 1 and early in interstadial OIC 3. The poorest matches occur in glacial periods, when local high-frequency, high-amplitude variations dominate [*Pahnke et al.*, 2003]. However, maximum cooling during the LGM occurs at 23–20 ka, similar to the timing of the SST minimum across the Indo-Pacific region at 20.5 ± 1.4 ka [*Barrows and Juggins*, 2005]. This coincides with minimum insolation at 22 ka. It is important to note that the same coincidence with insolation is present in the clastic and vegetation records as well. This indicates that the observation extends across both terrestrial and marine realms.

[45] Although the timing of major thermal events correlates with insolation maxima and minima, the response shape of the SST records differ markedly from that of insolation changes. The SST records from the warmer areas have the characteristic shape of a peak during OIC 5e, a cooler "plateau" during the rest of OIC 5, maximum cold in both OIC 4 and 2, and intermediate SST during OIC 3. This pattern resembles a composite carbon dioxide content record from the Vostok ice core (Figure 6) and supports the idea that temperature variations in the middle to low latitudes are occurring largely in tandem with changes in greenhouse gas content. Consequently, temperature change in the Southern Hemisphere driven by insolation changes is largely effected through the atmosphere. First-order temperature fluctuations follow atmospheric CO_2 (Figure 6), which is probably the major mechanism of global temperature synchronization. Overall, the carbon dioxide record and a stack of SST from SO136-GC3 (Figure 6) share 65% of the variance. It is important to note that in the Southern Ocean during OIC 5, cooling is initiated before carbon dioxide levels begin to decrease, indicating the presence of a second climate control mechanism here. Even taking this into account, the carbon dioxide record and the stack of SST from MD97-2120 and MD88-770 share 61% of the variance (Figure 6). The correlation here is lowered by millennial-scale variations in SST during OIC 3 that do not follow CO_2 variations. In Antarctica, the Vostok δD record [*Petit et al.*, 1999], explained mostly by temperature, shares a high 79% of the variance with the composite carbon dioxide record. This indicates thermal isolation of inland Antarctica from the Southern Ocean, the latter probably being the location of the millennial-scale variations. This is clearly seen in the differences in the shape of the Vostok ice core δD record [*Petit et al.*, 1999] and the more coastal ice core records like Byrd (Figure 7).

5.3. Rapid Climate Change and Suborbital Variation in Sea Surface Temperature

[46] Superimposed upon the major climate trends over the last 150,000 years are second-order fluctuations occurring on a millennial timescale that cannot be explained by variations in orbital parameters. These events are most clear during, and when entering and exiting OIC 3, periods of high terrestrial ice volume. These events are most pronounced in the Southern Ocean cores and are least visible in the lower-latitude core (SO136-GC3), which is dominated by trends over longer periods.

[47] The timing of the four most prominent warming events during OIC 3 is similar between the highest-resolution cores MD88-770 and MD97-2120. We plot the stack of these two records in Figure 7 together with the Byrd and GISP2 ice core δ^{18}O records [*Grootes et al.*, 1993; *Johnsen et al.*, 1972]. Over the interval 10,000 to 90,000 years, the Southern Ocean stack and the Byrd δ^{18}O record share 65% of the variance, signifying a close climatic link. The warming events in OIC 3 in the stack occur at 57.8, 51.8, 45.4, and 38.9 ka approximately 6000–7000 years apart. Considering the errors in our age models, the four OIC 3 events occur just before the Dansgaard-Oeschger (DO) events 17 (57.5 ka), 14 (51.6 ka), 12 (45.3 ka), and 8 (38.2 ka) in the GISP2 ice core [*Grootes et al.*, 1993]. *Blunier et al.* [1998] and *Blunier and Brook* [2001] observed that when Byrd and Vostok Antarctic ice cores were placed on the same timescale with the Greenland ice cores (GRIP and GISP2), events A1–A4 occurred at approximately the same time as DO events 17, 14, 12 and 8. *Pahnke et al.* [2003] and *Sachs and Anderson* [2005] showed that MD97-2120 records have elements very similar to both the Antarctic ice cores and to Greenland. Our comparison of the Southern Ocean SST stack with the ice cores illustrates that the common timing of these events appears to extend over the Australasian sector of the Southern Ocean.

[48] *Blunier et al.* [1998] and *Blunier and Brook* [2001] showed that warming before A1–A7 led the warming into their Northern DO counterparts by 1500–3000 years. *Brook et al.* [2005] confirmed this finding using both δ^{18}O of O_2 and methane in the Siple Dome ice core. The most pronounced warming leads observed by *Blunier and Brook* [2001] in the Byrd record were those starting A4, A2 and the deglaciation. These leads are well beyond potential errors in the matching of methane records or the gas closure time of the ice. Although our age models are not as precise as in ice cores, we observe similar leads of warming of SST in the Southern Ocean going into A1–A4 of 900 to 2500 years.

[49] Similar events to A1–A4 occur in many of the other proxy records. The presence of these events both in Antarctica and in multiple records of different nature near Australia and New Zealand indicates they are widespread features of climate change in the mid to high latitudes of the Southern Hemisphere. The similarity of the clastic record of DSDP site 594 (and the glacial record of Australia and New Zealand) with the Southern Ocean SST stack (65% shared variance) signifies close climatic links across this region between land and sea. Even across the Southern Ocean, 60% of the

Figure 5. MD97-2120. (a) SST record from Mg/Ca [*Pahnke et al.*, 2003]. (b) Alkenone concentration from *Sachs and Anderson* [2005]. (c) Sediment lightness (L*) from *Michel and Turon* [2006]. (d) Age model (triangles are radiocarbon dates with 1 σ error bars, and squares are oxygen isotope age tie points). Radiocarbon dates are from *Pahnke et al.* [2003]. Solid symbols were used to construct the age model. (e) Oxygen isotope record for *Gg. bulloides* [*Pahnke et al.*, 2003]. The line represents a three-point running mean.

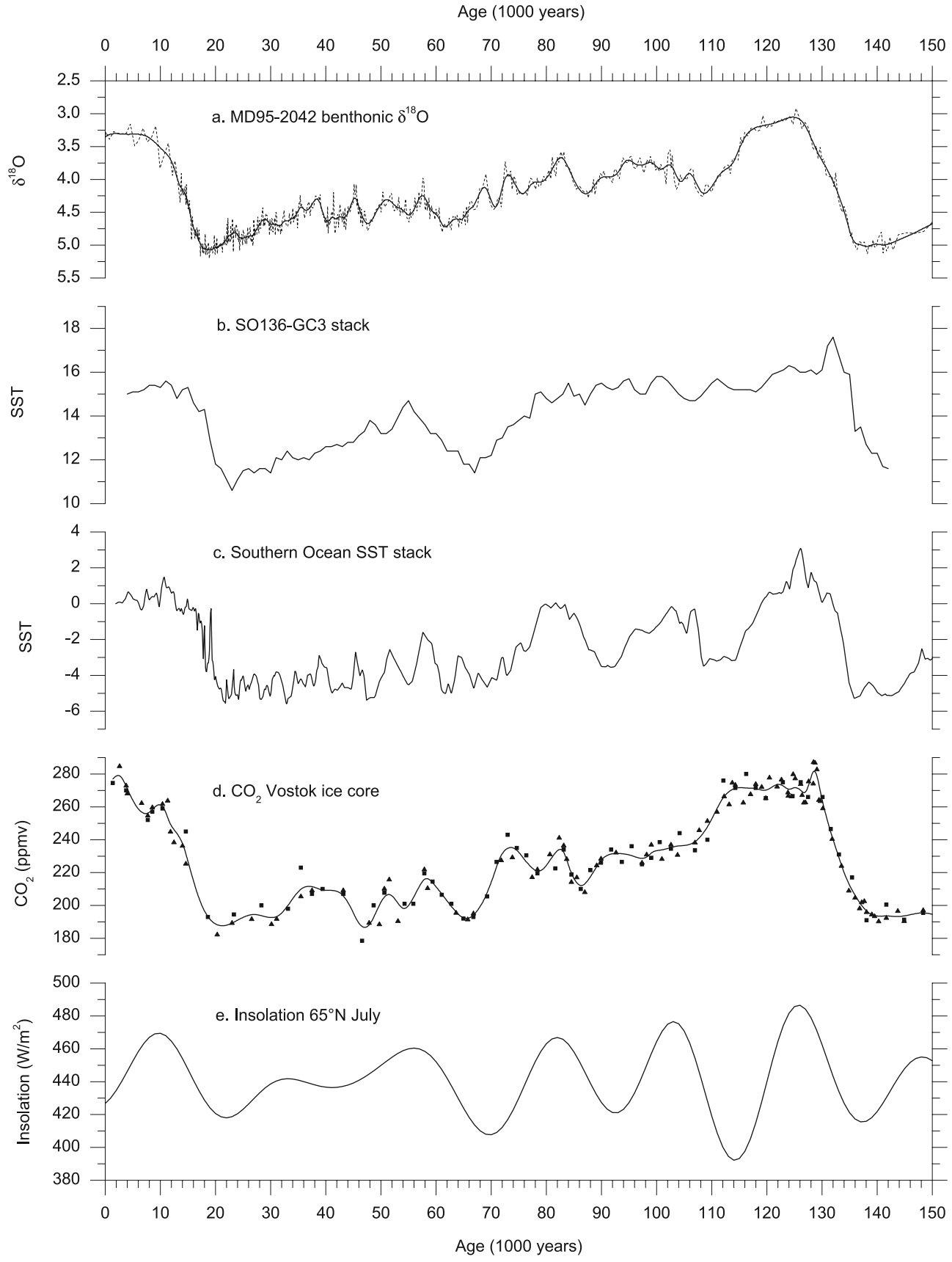
Age (1000 years)
a. MD95-2042 benthonic δ18O
δ18O
b. SO136-GC3 stack
SST
c. Southern Ocean SST stack
SST
d. CO2 Vostok ice core
CO2 (ppmv)
e. Insolation 65°N July
Insolation (W/m2)
Age (1000 years)

Figure 6

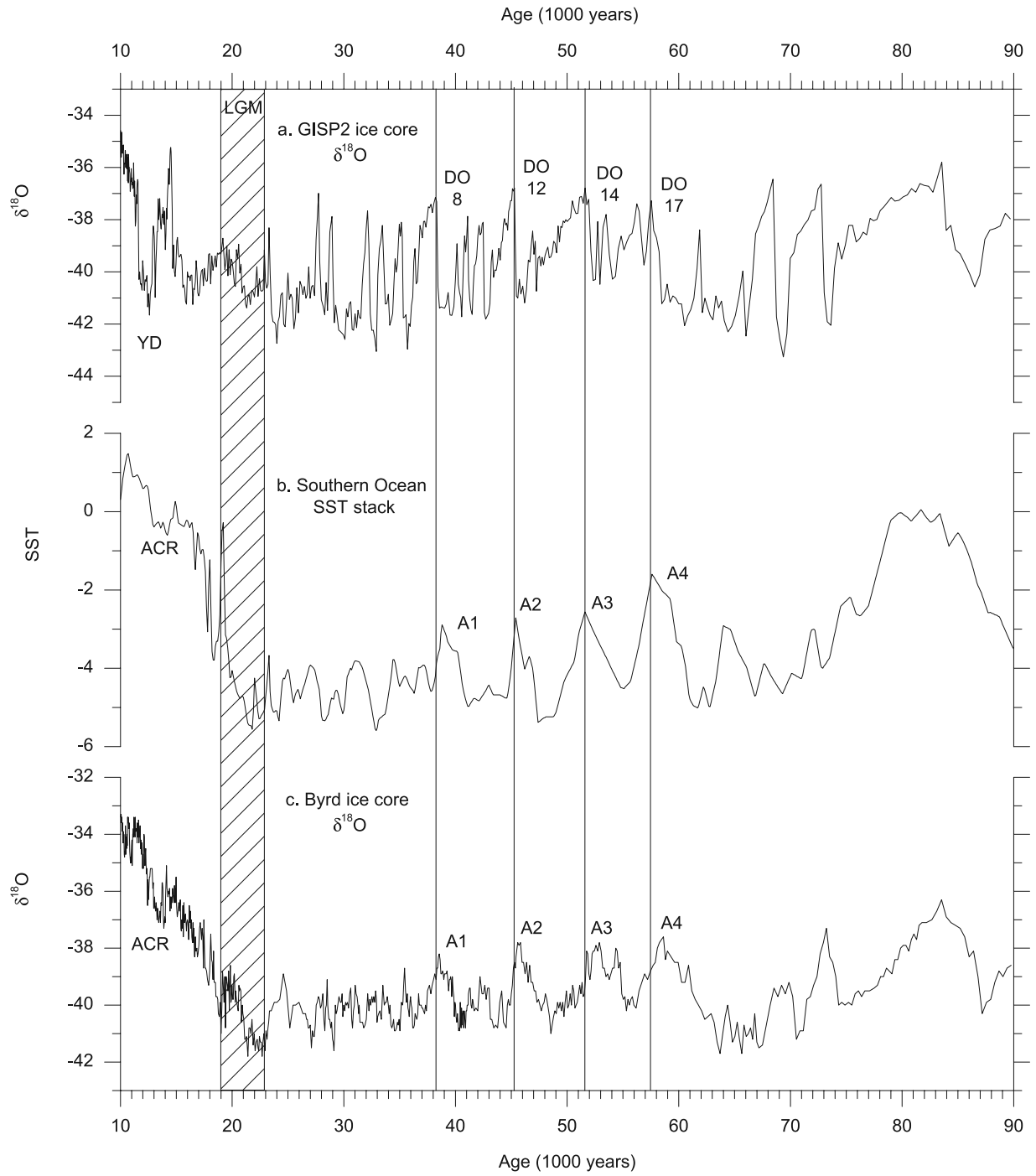

Figure 7. (a) GISP 2 oxygen isotope record [*Grootes et al.*, 1993] on the *Meese et al.* [1997] timescale. (b) Southern Ocean SST stack (see Figure 6). (c) Byrd ice core oxygen isotope record [*Johnsen et al.*, 1972] on the *Blunier and Brook* [2001] GISP2 timescale. Shaded zone signifies the Last Glacial Maximum (LGM) (19,000–23,000 years). YD is Younger Dryas chronozone; ACR is Antarctic Cold Reversal.

Figure 6. (a) MD95-2042 benthonic foraminifera oxygen isotope record (dashed line) [*Shackleton et al.*, 2004]. Thick line represents a spline fit of the data. (b) SO136-GC3 SST stack. This is a simple stack created by averaging the faunal-based and the $U^{K'}_{37}$ SST together. Both records were interpolated at 100-year intervals before stacking. (c) Southern Ocean SST stack. This is a simple stack created by averaging the MD97-2120 and MD88-770 SST records together. The resultant temperature was normalized to a "modern" value of 0°C. (d) CO_2 in the Vostok ice core. The curve represents a spline fit through the data of *Petit et al.* [1999] (triangles) and *Barnola et al.* [1987] (squares) on the VK-FGT1 timescale [*Parrenin et al.*, 2004]. (e) Insolation at 65°N for July [*Berger and Loutre*, 1991].

variance is shared between the Vostok temperature reconstruction over the last 150,000 years [*Petit et al.*, 1999] (on the VK-FGT1 timescale of *Parrenin et al.* [2004]) and the clastic record. This indicates that the temperature patterns we see in Antarctica and in the Southern Ocean are representative of the temperate latitudes of Australia and New Zealand. This also explains the synchroneity of the SST minimum across the Indo-Pacific region [*Barrows and Juggins*, 2005].

[50] The pattern of the last deglaciation in the Southern Hemisphere records differs markedly from that seen in the Northern Hemisphere (e.g., Figure 7). Postglacial warming of SST after the LGM is rapid in all cores, with the bulk of the warming occurring before 15 ka. It is important to note that Holocene-like temperatures are seen by 15 ka in all records. This rapid warming precedes warming at the base of the Bølling/Allerød chronozone in GISP2 by at least 3000–4000 years. The deglacial warming up to 15 ka is not monotonic in all cores, and in the highest-resolution record is punctuated by several temperature reversals, the first of which is the most distinct. These events are so brief that only the highest-resolution or most sensitive records, such as MD88-770 or mountain glaciation, are likely to preserve them. A temperature reversal is observed in the Byrd $\delta^{18}O$ record at 19.0 ka. Another similar, but less well dated, cold reversal occurs in the Taylor Dome record in close proximity to the Southern Ocean and its heat transport [*Steig et al.*, 1998]. The absence of this event in the continental Antarctic ice cores (such as the Vostok ice core) suggests it is a sensible heat phenomenon local to the Southern Ocean and areas under the meteorological influence of the Southern Ocean, such as southern Australia and New Zealand, and its effect diminishes with distance from this zone when greenhouse gas forcing becomes dominant.

[51] After 15 ka, there are no strong cooling events and any reversals in the warming trend are of a magnitude close to the error of the reconstructions. Therefore it is difficult to distinguish the Antarctic Cold Reversal but there is a cold reversal from 14.9 to 12.6 in the Southern Ocean SST stack that matches it in timing. A cooling period is absent during the Younger Dryas (YD) chronozone (11.6–12.9 ka given by *Meese et al.* [1997]) in the stack, which is composed of the best available records, where rapid climate change on short timescales is clearly demonstrated. Indeed, the YD is a time of warming in the stack. This matches observations from pollen data in New Zealand [*Turney et al.*, 2003]. This is in stark contrast to the YD seen in the Northern Atlantic Ocean, which is a pronounced and major return to glacial maximum conditions for ~1000 years (Figure 7). This adds further support to observations from the Antarctic ice cores that the YD event as such is not seen in the mid to high latitudes of the Southern Hemisphere and that a bipolar "seesaw" effect is in operation [*Broecker*, 1998].

[52] Last, it is important to note that the rapid SST changes in MD88-770 and MD97-2120 through OIC 3 are too rapid to be explained by atmospheric greenhouse gas forcing. Therefore these shifts indicate rapid changes in the distribution of sensible heat at the surface of the Southern Ocean. The most likely cause of this is a major meridional rearrangement of isotherms associated with surface circulation. The rate and magnitude of SST change associated with these shifts is of a nature typically attributed to Polar Front shifts in the North Atlantic Ocean [*CLIMAP Project Members*, 1981]. Input of heat from western boundary currents (such as the Agulhas Current and East Australian Current "heat pumps") and export of heat in eastern boundary currents [*Tomczak and Godfrey*, 1994] must have significantly changed the heat budget of the Southern Ocean on millennial timescales. It is also likely that changing wind fields over the Southern Ocean played a pivotal role in redistributing this heat [*Shulmeister et al.*, 2004].

[53] **Acknowledgments.** T.T.B. thanks Scott Lehman for his hospitality during his stay at INSTAAR, University of Colorado. We thank Judith Shelley, who provided invaluable assistance preparing samples, and Michelle Spooner, who performed some of the planktonic foraminifera counting. We thank Heather Scott-Gagan, Joseph Cali, and Michael Gagan (Research School of Earth Sciences, ANU) for helping to prepare the oxygen isotope data. Graham Logan is acknowledged for providing the opportunity and facilities to work at Geoscience Australia. P.D.D. received Australian Research Council funding for work on SO136-GC3. Jörn Thiede and Stefan Nees provided access to the cores and facilitated the radiocarbon dating. Arne Sturm and Gerrit J. van der Lingen kindly provided access to unpublished data. E.C. and C.P. also acknowledge a Ramon y Cajal contract from the Spanish Ministry of Education and Science.

References

Alley, R. B., and P. U. Clark (1999), The deglaciation of the Northern Hemisphere: A global perspective, *Annu. Rev. Earth Planet. Sci.*, *27*, 149–182.

Bard, E. (1988), Correction of accelerator mass spectrometry dates measured in planktonic foraminifera: Paleoceanographic implications, *Paleoceanography*, *3*, 635–645.

Bareille, G., F. E. Grousset, and M. Labracherie (1994), Origin of detrital fluxes in the southeast Indian Ocean during the last climatic cycles, *Paleoceanography*, *9*, 799–819.

Barnola, J. M., D. Raynaud, Y. S. Korotkevich, and C. Lorius (1987), Vostok ice core provides 160,000-year record of atmospheric CO_2, *Nature*, *329*, 408–414.

Barrows, T. T., and S. Juggins (2005), Sea-surface temperatures around the Australian margin and Indian Ocean during the Last Glacial Maximum, *Quat. Sci. Rev.*, *24*, 1017–1047.

Barrows, T. T., S. Juggins, P. De Deckker, J. Thiede, and J. I. Martinez (2000), Sea-surface temperatures of the southwest Pacific Ocean during the last glacial maximum, *Paleoceanography*, *15*, 95–109.

Barrows, T. T., J. O. Stone, L. K. Fifield, and R. G. Cresswell (2001), Late Pleistocene glaciation of the Kosciuszko Massif, Snowy Mountains, Australia, *Quat. Res.*, *55*, 179–189.

Barrows, T. T., J. O. Stone, L. K. Fifield, and R. G. Cresswell (2002), The timing of the Last Glacial Maximum in Australia, *Quat. Sci. Rev.*, *21*, 159–173.

Barrows, T. T., J. O. Stone, and L. K. Fifield (2004), Exposure ages for Pleistocene periglacial deposits in Australia, *Quat. Sci. Rev.*, *23*, 697–708.

Berger, A., and M. F. Loutre (1991), Insolation values for the climate of the last 10 million years, *Quat. Sci. Rev.*, *10*, 297–317.

Black, K. P., C. S. Nelson, and C. H. Hendy (1988), A spectral analysis procedure for dating Quaternary deep-sea cores and its application to a high-resolution Brunhes record from the southwest Pacific, *Mar. Geol.*, *83*, 21–30.

Blunier, T., and E. J. Brook (2001), Timing of millennial-scale climate change in Antarctica and Greenland during the last glacial period, *Science*, *291*, 109–112.

Blunier, T., et al. (1998), Asynchrony of Antarctic and Greenland climate change during the last glacial period, *Nature*, *394*, 739–743.

Broecker, W. S. (1998), Paleocean circulation during the last deglaciation: A bipolar seesaw?, *Paleoceanography*, *13*, 119–121.

Brook, E. J., J. W. C. White, A. S. M. Schilla, M. L. Bender, B. Barnett, J. P. Severinghaus, K. C. Taylor, R. B. Alley, and E. J. Steig (2005), Timing of millennial-scale climate change at Siple Dome, West Antarctica, during the last glacial period, *Quat. Sci. Rev.*, *24*, 1333–1343.

Chapronière, G. C. H. (1991), Pleistocene to Holocene planktic foraminiferal biostratigraphy of the Coral Sea, offshore Queensland, Australia, *BMR J. Aust. Geol. Geophys.*, *12*, 195–221.

CLIMAP Project Members (1981), Seasonal reconstructions of the Earth's surface at the Last Glacial Maximum, *Geol. Soc. Am. Map Chart Ser., MC-36*.

Duplessy, J. C., E. Bard, M. Arnold, N. J. Shackleton, J. Duprat, and L. Labeyrie (1991), How fast did the ocean-atmosphere system run during the last deglaciation?, *Earth Planet. Sci. Lett.*, *103*, 27–40.

Elderfield, H., and G. Ganssen (2000), Past temperature and $\delta^{18}O$ of surface ocean waters inferred from foraminiferal Mg/Ca ratios, *Nature*, *405*, 442–445.

Grootes, P. M., M. Stuiver, J. W. C. White, S. Johnsen, and J. Jouzel (1993), Comparison of oxygen isotope records from the GISP2 and GRIP Greenland ice cores, *Nature*, *366*, 552–554.

Hays, J. D., J. Imbrie, and N. J. Shackleton (1977), Variations in the Earth's orbit: Pacemaker of the ice ages?, *Science*, *198*, 529–530.

Hemleben, C., M. Spindler, and O. R. Anderson (1989), *Modern Planktonic Foraminifera*, 363 pp., Springer, New York.

Heusser, L. E., and G. Van de Geer (1994), Direct correlation of terrestrial and marine paleoclimatic records from four glacial-interglacial cycles—DSDP site 594 southwest Pacific, *Quat. Sci. Rev.*, *13*, 273–282.

Howard, W. R., and W. L. Prell (1992), Late Quaternary surface circulation of the southern Indian Ocean and its relationship to orbital variations, *Paleoceanography*, *7*, 79–117.

Imbrie, J., et al. (1992), On the structure and origin of major glaciation cycles: 1. Linear responses to Milankovich forcing, *Paleoceanography*, *7*, 701–738.

Johnsen, S. J., H. B. Clausen, W. Dansgaar, and C. C. Langway (1972), Oxygen isotope profiles through Antarctic and Greenland ice sheets, *Nature*, *235*, 429–434.

Kennett, J. P., and M. S. Srinivasan (1983), *Neogene Planktonic Foraminifera: A Phylogenetic Atlas*, John Wiley, Hoboken, N. J.

Kershaw, A. P., J. Tibby, D. Penny, H. Yezdani, R. Walkley, E. J. Cook, and R. Johnston (2004), Latest Pleistocene and Holocene vegetation and environmental history of the western plains of Victoria, *Proc. R. Soc. Vict.*, *116*, 141–163.

Labeyrie, L., et al. (1996), Hydrographic changes of the Southern Ocean (southeast Indian sector) over the last 230 kyr, *Paleoceanography*, *11*, 57–76.

Lea, D. W., D. K. Pak, and H. J. Spero (2000), Climate impact of late Quaternary equatorial Pacific sea surface temperature variations, *Science*, *289*, 1719–1724.

Martinez, J. I., P. De Deckker, and T. T. Barrows (1999), Palaeoceanography of the last glacial maximum in the eastern Indian Ocean: Planktonic foraminiferal evidence, *Palaeogeogr. Palaeoclimatol. Palaeoecol.*, *147*, 73–99.

Martinez, J. I., P. De Deckker, and T. T. Barrows (2002), Palaeoceanography of the western Pacific Warm Pool during the last glacial maximum - of significance to long term monitoring of the maritime continent, in *Environmental and Human History and Dynamics of the Australian Southeast Asian Region*, edited by P. Bishop, A. P. Kershaw, and N. Tapper, *Adv. Geoecol.*, *34*, 147–172.

Martinson, D. G., N. G. Pisias, J. D. Hays, J. Imbrie, T. C. Moore Jr. and N. J. Shackleton (1987), Age dating and the orbital theory of the ice ages: Development of a high-resolution 0 to 30,0000-year chronostratigraphy, *Quat. Res.*, *27*, 1–29.

Mashiotta, T. A., D. W. Lea, and H. J. Spero (1999), Glacial-interglacial changes in subantarctic sea surface temperature and $\delta^{18}O$-water using foraminiferal Mg, *Earth Planet. Sci. Lett.*, *170*, 417–432.

Matsumoto, K., and R. M. Key (2004), Natural radiocarbon distribution in the deep ocean, in *Global Environmental Change in the Ocean and on Land*, edited by M. Shiyomi et al., pp. 45–58, Terra Sci., Tokyo.

Meese, D. A., A. J. Gow, R. B. Alley, G. A. Zielinski, P. M. Grootes, M. Ram, K. C. Taylor, P. A. Mayewski, and J. F. Bolzan (1997), The Greenland Ice Sheet Project 2 depth-age scale: Methods and results, *J. Geophys. Res.*, *102*, 26,411–26,423.

Michel, E., and J.-L. Turon (2006), Reflectance of sediment core MD97–2120, http://www.pangaea.de/, doi:10.1594/PANGAEA.509434, PANGAEA, Network for Geosci. and Environ Data, Bremerhaven, Germany.

Morley, J. J. (1989), Variations in high-latitude fronts in the southern Indian Ocean: An estimation based on faunal changes, *Paleoceanography*, *4*, 547–554.

Müller, P. J., G. Kirst, G. Ruhland, I. von Storch, and A. Roselle-Mele (1998), Calibration of the alkenone paleotemperature index $U^{K'}37$ based on core-tops from the eastern South Atlantic and the global ocean (60°N–60°S), *Geochim. Cosmochim. Acta*, *62*, 1757–1772.

Nelson, C. S., P. J. Cooke, C. G. Hendy, and A. M. Cuthbertson (1993), Oceanographic and climatic changes over the past 160,000 years at Deep Sea Drilling Project Site 594 off southwestern New Zealand, southwest Pacific Ocean, *Paleoceanography*, *8*, 435–458.

Nelson, C. S., C. H. Hendy, and A. M. Cuthbertson (1994), Oxygen-isotope evidence for climatic contrasts between Tasman Sea and southwest Pacific Ocean during the late Quaternary, in *Evolution of the Tasman Sea Basin*, edited by G. J. van der Lingen, K. M. Swanson, and R. J. Muir, pp. 181–196, A. A. Balkema, Rotterdam, Netherlands.

Pahnke, K., and R. Zahn (2005), Southern Hemisphere water mass conversion linked with North Atlantic climate variability, *Science*, *307*, 1741–1746.

Pahnke, K., R. Zahn, H. Elderfield, and M. Schulz (2003), 340,000-year centennial-scale marine record of Southern Hemisphere climatic oscillation, *Science*, *301*, 948–952.

Parrenin, F., F. Rémy, C. Ritz, M. J. Siegert, and J. Jouzel (2004), New modeling of the Vostok ice flow line and implication for the glaciological chronology of the Vostok ice core, *J. Geophys. Res.*, *109*, D20102, doi:10.1029/2004JD004561.

Pelejero, C., E. Calvo, G. A. Logan, and P. De Deckker (2003), Marine isotopic stage 5e in the southwest Pacific: Similarities with Antarctica and ENSO inferences, *Geophys. Res. Lett.*, *30*(23), 2185, doi:10.1029/2003GL018191.

Pelejero, C., E. Calvo, T. T. Barrows, G. A. Logan, and P. De Deckker (2006), South Tasman Sea alkenone paleothermometry over the last four glacial/interglacial cycles, *Mar. Geol.*, *230*, 73–86.

Petit, J. R., et al. (1999), Climate and atmospheric history of the past 420,000 years from the Vostok ice core, Antarctica, *Nature*, *399*, 429–436.

Pisias, N. G., D. G. Martinson, T. C. Moore Jr., N. J. Shackleton, W. Prell, J. Hays, and G. Boden (1984), High resolution stratigraphic correlation of benthic oxygen isotopic records spanning the last 300,000 years, *Mar. Geol.*, *56*, 119–136.

Prahl, F. G., L. A. Muehlhausen, and D. L. Zahnle (1988), Further evaluation of long-chain alkenones as indicators of paleoceanographic conditions, *Geochim. Cosmochim. Acta*, *52*, 2303–2310.

Prell, W. L., J. Imbrie, D. G. Martinson, J. J. Morley, N. G. Pisias, N. J. Shackleton, and H. F. Streeter (1986), Graphic correlation of oxygen-isotope stratigraphy: Application to the late Quaternary, *Paleoceanography*, *1*, 137–162.

Sachs, J. P., and R. F. Anderson (2005), Increased productivity in the subantarctic ocean during Heinrich events, *Nature*, *434*, 1118–1121.

Saito, T., P. R. Thompson, and D. Breger (1981), *Systematic Index of Recent and Pleistocene Planktonic Foraminifera*, 190 pp., Univ. of Tokyo Press, Tokyo.

Shackleton, N. J., R. G. Fairbanks, T.-C. Chiu, and F. Parrenin (2004), Absolute calibration of the Greenland time scale: Implications for Antarctic time scales and for $\Delta^{14}C$, *Quat. Sci. Rev.*, *23*, 1513–1522.

Shulmeister, J., et al. (2004), The Southern Hemisphere westerlies in the Australasian sector over the last glacial cycle: A synthesis, *Quat. Int.*, *118–119*, 23–53.

Sikes, E. L., W. R. Howard, H. L. Neil, and J. K. Volkman (2002), Glacial-interglacial sea surface temperature changes across the subtropical front east of New Zealand based on alkenone unsaturation ratios and foraminiferal assemblages, *Paleoceanography*, *17*(2), 1012, doi:10.1029/2001PA000640.

Skinner, L. C., and N. J. Shackleton (2005), An Atlantic lead over Pacific deep-water change across termination I: Implications for the application of the marine isotope stage stratigraphy, *Quat. Sci. Rev.*, *24*, 571–580.

Steig, E. J., E. J. Brook, J. W. C. White, C. M. Sucher, M. L. Bender, S. J. Lehman, D. L. Morse, E. D. Waddington, and G. D. Clow (1998), Synchronous climate changes in Antarctica and the North Atlantic, *Science*, *282*, 92–95.

Stuiver, M., P. J. Reimer, E. Bard, J. W. Beck, G. S. Burr, K. A. Hughen, B. Kromer, F. G. McCormac, J. van der Plicht, and M. Spurk (1998), INTCAL98 radiocarbon age calibration, 24,000–0 cal BP, *Radiocarbon*, *40*, 1041–1083.

Suggate, R. P. (1990), Late Pliocene and Quaternary glaciations of New Zealand, *Quat. Sci. Rev.*, *9*, 175–197.

Suggate, R. P., and P. C. Almond (2005), The Last Glacial Maximum (LGM) in western South Island, New Zealand: Implications for

the global LGM and MIS 2, *Quat. Sci. Rev.*, *24*, 1923–1940.

Telford, R. J., and H. J. B. Birks (2005), The secret assumption of transfer functions: Problems with spatial autocorrelation in evaluating model performance, *Quat. Sci. Rev.*, *24*, 2173–2179.

Thiede, J., and S. Nees (1999), FS SONNE cruise report SO136 TASQWA, 62 pp., *Rep. 69*, GEOMAR, Kiel, Germany.

Tomczak, M., and J. S. Godfrey (1994), *Regional Oceanography: An Introduction*, 422 pp., Elsevier, New York.

Turney, C. S. M., M. S. McGlone, and J. M. Wilmshurst (2003), Asynchronous climate change between New Zealand and the North Atlantic during the last deglaciation, *Geology*, *31*, 223–226.

Vandergoes, M. J., R. M. Newnham, F. Preusser, C. H. Hendy, T. V. Lowell, S. J. Fitzsimons, A. G. Hogg, H. U. Kasper, and C. Schluchter (2005), Regional insolation forcing of late Quaternary climate change in the Southern Hemisphere, *Nature*, *436*, 242–245.

Waelbroeck, C., L. Labeyrie, J.-C. Duplessy, J. Guiot, M. Labracherie, H. Leclaire, and J. Duprat (1998), Improving past sea surface temperature estimates based on planktonic fossil faunas, *Paleoceanography*, *13*, 272–283.

Weaver, P. P. E., L. Carter, and H. Neil (1998), Response of surface water masses and circulation to late Quaternary climate change east of New Zealand, *Paleoceanography*, *13*, 70–83.

Wells, P., and O. Okada (1997), Response of nannoplankton to major changes in sea-surface temperature and movements of hydrological fronts over Site DSDP 594 (south Chatham Rise, southeastern New Zealand), during the last 130 kyr, *Mar. Micropaleontol.*, *32*, 341–363.

Wells, P. E., and G. M. Wells (1994), Large-scale reorganization of ocean currents offshore Western Australia during the late Quaternary, *Mar. Micropaleontol.*, *24*, 157–186.

Williams, D. F. (1976), Late Quaternary fluctuations of the polar front and subtropical convergence in the southeast Indian Ocean, *Mar. Micropaleontol.*, *1*, 363–375.

T. T. Barrows, Department of Nuclear Physics, Australian National University, Canberra, ACT 0200, Australia. (tim.barrows@anu.edu.au)

E. Calvo, Institut de Ciències del Mar, CMIMA-CSIC, Pg. de la Barceloneta 37, E-08003 Barcelona, Spain.

P. De Deckker, Department of Earth and Marine Sciences, Australian National University, Canberra, ACT 0200, Australia.

S. Juggins, School of Geography, Politics and Sociology, University of Newcastle, Newcastle upon Tyne, NE1 7RU UK.

C. Pelejero, Institució Catalana de Recerca i Estudis Avançats (ICREA), CMIMA-CSIC, Pg. de la Barceloneta 37, E-08003 Barcelona, Spain.